Analyst

ROYAL SOCIETY OF CHEMISTRY

PAPER

View Article Online
View Journal

Cite this: DOI: 10.1039/d1an00455g

On-demand lactate monitoring towards assessing physiological responses in sedentary populations†

Ashlesha Bhide,[a] Kai-Chun Lin,[a] Sriram Muthukumar[b] and Shalini Prasad*[a]

Identification of diseases in sedentary populations on a timely basis before reaching a critical stage is a continuing challenge faced by emergency care centers. Lactate is a key biomarker for monitoring restricted oxygen supply essential for assessing the physiological responses of the user for clinical diagnostics. The novelty of this work is the development of a non-invasive, mediator-free, stick and remove biosensor for the on-demand measurement of lactate in passive sweat targeted towards sedentary populations. The conformable interface of the biosensors with skin can be engineered to extract relevant biochemical signals and quantify the *in situ* sweat biomarker levels. In this work, we demonstrate a highly sensitive and specific on-demand biosensor with a fabricated hybrid nanotextured Au/ZnO electrode stack embedded within a flexible nanoporous material to capture the temporal dynamics of passive sweat lactate. The biosensor exhibits a lactate specific response in human sweat with a 1 mM lower limit of detection and a wide dynamic detection range of 1–100 mM (R^2 = 0.98). The proposed biosensor has a sensitivity of 8.3% mM^{-1} while selectivity studies reveal negative interactions with non-specific molecules. The sensor stability studies showed an ~30% degradation in the lactate biosensing response over a 4-day duration when stored at 4 °C. Non-faradaic electrochemical spectroscopy is employed as the detection modality to quantify the enzymatic catalysis of sweat lactate at the electrode–sweat interface. Spectroscopic characterization techniques such as XPS, ATR–FTIR, and zeta potential measurements confirm the enzymatic assay binding efficacy on a qualitative scale.

Received 16th March 2021,
Accepted 5th April 2021

DOI: 10.1039/d1an00455g

rsc.li/analyst

1. Introduction

Geriatric and paediatric populations are vulnerable to unforeseen circumstances that demand the identification of technologies that can prolong the lives of these sedentary population subsets. Thus, facile care approaches are required to monitor the health parameters of sedentary populations calling for the need of developing on-demand, single-use platforms for point-of-use testing. Early screening and diagnosis provide initial heath intervention through safe, non-invasive, and potentially inexpensive methods for detecting the onset and progression of diseases. Progression of diseases into an advanced stage causes delay in procuring effective treatment consequently requiring laborious invasive, immunological, imaging, and genomic diagnosis procedures.[1] The invasiveness of conventional diagnosis techniques requires frequent painful testing procedures posing a challenge for regular screening of disease progression in elderly and infants. Biomarkers have the enormous ability to assess and characterize the extent of disease towards the development of next-gen non-invasive diagnostic devices without the requirement of expensive and bulky equipment.[2] An increase in blood lactate levels is related to increased production or decreased lactate clearance further leading to conditions such as tissue hypoxia and subsequently leading to septic shock under extreme conditions.[3] Hence, an on-demand, point-of-use, stick and remove biosensor can be used for the initial quantification of lactate levels further prompting clinicians to initiate immediate medical actions.

For years, eccrine sweat has been a neglected diagnostic bodily fluid but with the advent of flexible sensing, sweat sampling has become an extremely promising non-invasive diagnostic approach for biomarker analysis. Most efforts have been focused on the detection of sweat metabolites such as lactate, glucose, and uric acid as they are present in higher detectable concentrations while the protein concentrations are in lower ranges. Low tonicity and acidic pH of sweat allow for more accumulation of biomarkers in sweat.[4] Eccrine sweat is a valuable source of proteins, metabolites, electrolytes, lipids, and other non-invasive biomarkers with less susceptibility to fouling making it a critical tool for frequent monitoring of disease states in sedentary populations.[5] Sweating occurs as a response to maintain thermoregulation when there is an

[a]Department of Bioengineering, University of Texas at Dallas, Richardson, TX-75080, USA. E-mail: Shalini.Prasad@utdallas.edu
[b]EnLisense LLC, 1813 Audubon Pond Way, Allen, TX, 75013, USA

†Electronic supplementary information (ESI) available. See DOI: 10.1039/d1an00455g

excess rise in the core body temperature. Higher sweat volumes can be achieved by inducing sweating through stimulation in healthy subjects. The quality and quantity of the biomarkers are highly dependent on the types of glands and the region of sweat sampling on the body. Eccrine sweat is present on the body's skin with an average density of 100–200 cm^{-2} on the surface area of the body with its appearance on the body's surface allowing for non-invasive biomarker detection.[6] Advancement in passive sweat sampling and iontophoretic sweat stimulation techniques has unlocked new opportunities for sweat analytics-based screening devices with the potential to provide continuous feedback on the health and disease status. Lactate levels in eccrine sweat are found to be higher than those in the blood ranging from 425 mM in healthy individuals to 50–100 mM after exhaustive exercise making sweat lactate detection a viable alternative for monitoring clinical conditions.[7–10] Most sweat based sensors rely on the localized pilocarpine stimulation of sweat glands so as to achieve 10–100 μL of sweat volume required for biomarker detection.[11,12] Studies have shown that sweat stimulation induced using pilocarpine did not significantly show a change in lactate levels before exercise and during exercise in the exercise group in comparison with the non-exercising group.[13] Previously, our group has demonstrated dynamic continuous monitoring of lactate in ultra-low volumes of passive perspired sweat on a graphene biosensing platform.[14] Recent studies have shown that real-time lactate biosensing requires high sweat volumes and the use of redox mediators to widen its dynamic range of detection[12,15–20] (see ESI Table S1†). Most of the efforts report a dynamic range up to ~70 mM with the use of redox probes. However, in our work, we report a non-faradaic, mediator-free lactate sensing strategy with an extended dynamic detection range up to 100 mM by leveraging the properties of a porous substrate.

Porous substrates such as polyamide offer higher current density and capacitance due to their enlarged surface area to volume ratio in comparison with flat substrates. The dimensionality of the electrode materials also enhances the kinetics of electrochemical reactions.[21] Nanoporous membranes allow for nanoconfinement of biomolecules within small volumes to increase the frequency of interactions with the biomolecules and the functionalized electrode surface. The sensitivity of biomarkers can be enhanced by macromolecular crowding in the nanopores which influences the conformal stability of the protein, enhances the folding process, accelerates enzyme reaction kinetics, and prevents protein denaturation.[22] The specificity in detecting the target biomarker is achieved by the excluded-volume effect wherein the inert macromolecules crowd the nanopore and reduce the randomness in the motion of the target biomolecules.[23] A decrease in the entropy of a crowded solution increases the thermodynamic activity of the solution resulting from the volume exclusion effect thus allowing specific probe–target analyte interactions.[24] Aside from the biocompatibility provided by the polyamide required for integration in flexible devices, another important aspect of using porous substrates is their capability to capture ultralow sweat volumes, drive the passively produced local sweat from the epidermis to the functionalized electrode interface, and provide the user with instantaneous feedback. Experimental studies and simulation carried out previously by the group have shown that passive eccrine sweat is transported rapidly through the entire cross-section of the polyamide substrate steadily within 30 seconds in a radial profile through capillary action.[25]

Zinc oxide nanostructures have been explored extensively in recent years for biosensing applications (glucose, H_2O_2, and cholesterol) because they offer advantages such as faster response time and sensitivity of detection. The nanotextured surface of ZnO provides a greater surface area of probe–target biomarker interaction, biocompatibility, structural and chemical stability, fast electron kinetics, and strong adsorption ability due to its high isoelectric point.[26] The direct charge tunnelling between the ZnO nanostructures and the active site of the enzyme reduces the need to use a redox mediator.[27] The ZnO surface is positively charged at physiological pH allowing for immobilization of negatively charged proteins to be adsorbed on its surface by electrostatic forces of attraction.[28] The electronic properties of ZnO allow for the sensitive detection of biomarkers in small volumes with a wider dynamic range of detection while tailoring the polar termination of the ZnO surface enhances the selectivity of the biosensor. The zinc and oxygen terminations of the ZnO nanostructures have been demonstrated to be efficient for the functionalization of antibodies and enzymes through dithiobis succinimidyl propionate (DSP) linker chemistry.[29] This work demonstrates the operation of a biosensor with the capability of providing an on-demand measurement to the user for monitoring elevated lactate levels. Highly sensitive and specific lactate detection is accomplished by capitalizing on the interaction between the low volumes of passive sweat entrapped in the pores of the substrate and the nanotextured hybrid Au/ZnO electrodes aiding in signal amplification for ultra-sensitive lactate detection.

2. Results and discussion

2.1. Enzymatic assay functionalization and structural characterization of the biosensing substrate

Lactate detection in eccrine sweat is achieved by the catalytic oxidation of L-lactate into pyruvic acid and H_2O_2 through lactate oxide (LOx) embedded within the nanopores and immobilized on the nanostructured ZnO active sensing region by a crosslinker as shown in Fig. 1a. The production of H_2O_2 contributes to the impedance changes which are monitored by electrochemical impedance spectroscopy. The fluid wicking profile of the nanoporous substrate in contact with 3 μL of passive sweat is shown in Fig. 1b. The sweat is introduced into the pores through the face opposite to the sensing region and is transported through the pores to interact with the enzyme. The mechanism guiding the fluid transport is a function of pore diameter, thickness, contact angle, packing density and

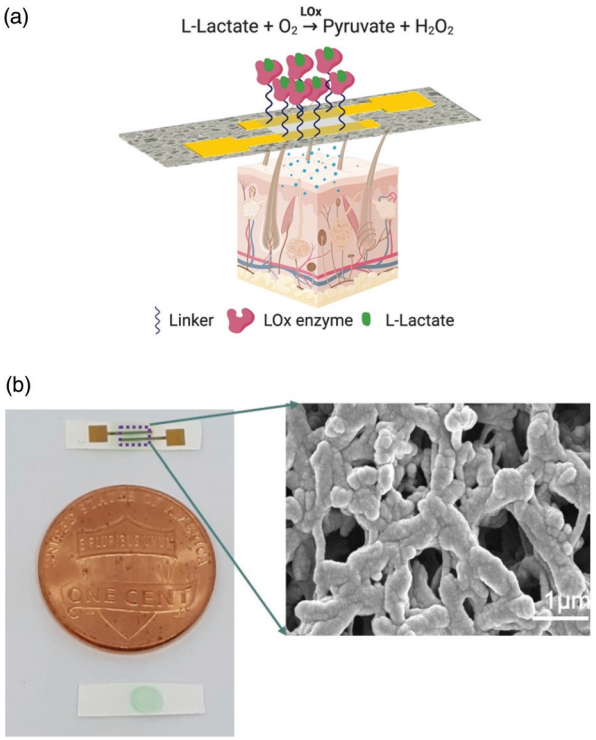

Fig. 1 (a) Enzymatic assay chemistry immobilized on the ZnO active sensing region for the detection of L-lactate. Created with BioRender.com. (b) Fluid wicking profile of the nanoporous polyamide substrate. The inset shows the SEM image of the substrate.

pore arrangement which drives the transport of sweat across the membrane and influences the biosensor metrics. The SEM image in the inset provides evidence for the intercalated pore structure that aids in the navigation of the passive sweat expressed from the epidermis to the detection region by lateral diffusion.

2.2. ATR–FTIR analysis for the confirmation of enzymatic assay functionalization on the lactate biosensing platform

Attenuated total reflectance spectroscopy provides detailed insight into the protein interactions occurring at the electrode–electrolyte interface. The interactions between the various layers of the enzymatic assay chemistry are characterized by a unique spectral fingerprint which is associated with the appearance or shift in certain absorption peaks. The ATR–FTIR spectra of the nanostructured ZnO surface modified with DSP and DSP–LOx chemistry within the spectral range of 600–4000 cm^{-1} are shown in Fig. 2a and b, respectively. The peak related to the ZnO nanotextured surface appears at 587 cm^{-1} and is shown in ESI Fig. S1b.† The DSP linker is an amine-reactive crosslinker consisting of NHS–ester groups at the ends of its spacer arm and a cleavable disulfide bond. The peaks appearing at 670 cm^{-1} and 705 cm^{-1} represent the vibrations of the CH_2 bond that form the backbone of DSP. The peaks at 1022 cm^{-1} and 1315 cm^{-1} are assigned to the stretching vibrations of the ester linkage and the symmetric C–

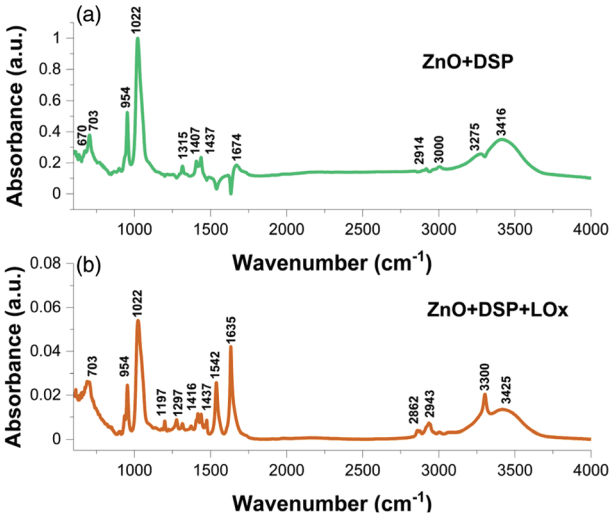

Fig. 2 (a) ATR–FTIR spectra of ZnO–linker (DSP) binding; (b) ZnO–linker (DSP)–enzyme (LOx) binding.

N–C stretch of NHS present in DSP, respectively. Other significant identifier groups present in DSP appear at 1674 cm^{-1} representing the asymmetric carbonyl stretch of the NHS ester group. The absorption bands at 1407 cm^{-1} and 1438 cm^{-1} are characteristics of the vibrations of the methylene scissors present in DSP. The bending vibrations of the alkane stretch (C–H) are indicated by the two peaks at 2915 cm^{-1} and 3000 cm^{-1}. The DSP linker binds to the enzyme at the NHS end by breaking the C=O bond to form a stable amide bond and releasing the succinimidyl group. This process is indicated by the appearance of peaks at 1020 cm^{-1} (C–N stretch) and 1200 cm^{-1} (C–C stretch) associated with the aminolysis of NHS groups in DSP with primary amines in the enzyme. The peak at 1044 cm^{-1} indicates the C–O vibrations in LOx. The peaks at 1633 cm^{-1} and 1538 cm^{-1} indicate the presence of amide I and amide II bonds of LOx. The amide I band appears due to the C–O stretching of the peptide linkage present in the backbone of the protein. The amide II band appears due to the combined stretching of the N–H and C–N bonds of the peptide group.

Another surface analysis technique called X-ray photoelectron spectroscopy is utilized to gain an in-depth understanding of the elemental composition of the interface being probed. XPS analysis was performed to ensure the binding of the thiol crosslinker to the sensing element. Fig. 3a–c show the XPS spectra of bare ZnO and the DSP modified ZnO surface for the Zn 2p3/2, O 1s, and N 1s peaks, respectively. The Zn 2p3/2 peak for bare ZnO appears at 1021.4 eV; it shifts to 1021.8 eV for the DSP modified ZnO surface indicating the formation of Zn–S bonds. The O 1s peak for bare ZnO observed at 530.8 eV shifts to 531.4 eV and can be attributed to the C=O group of the NHS terminus. The peak appearing at 533.4 eV indicates the presence of C–O in the NHS terminus of DSP. The N 1s peak appears at a binding energy of 400.4 eV after modifying the ZnO surface with DSP which is a signature of the nitrogen species present in the NHS ester.

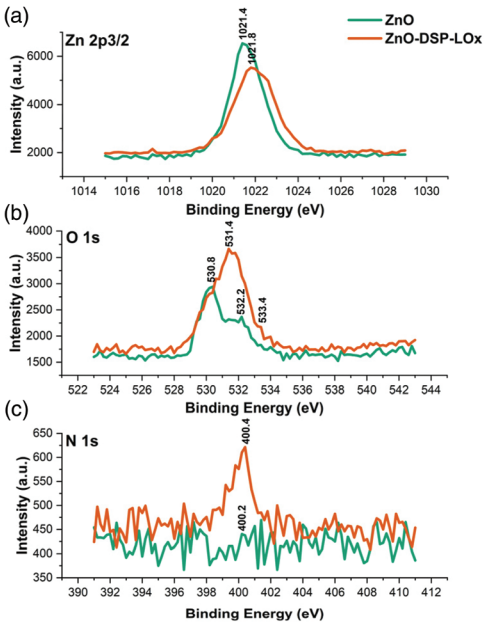

Fig. 3 XPS spectra of the bare ZnO and linker (DSP) modified ZnO surface for (a) Zn 2p3/2 peak, (b) O 1s peak and (c) N 1s peak.

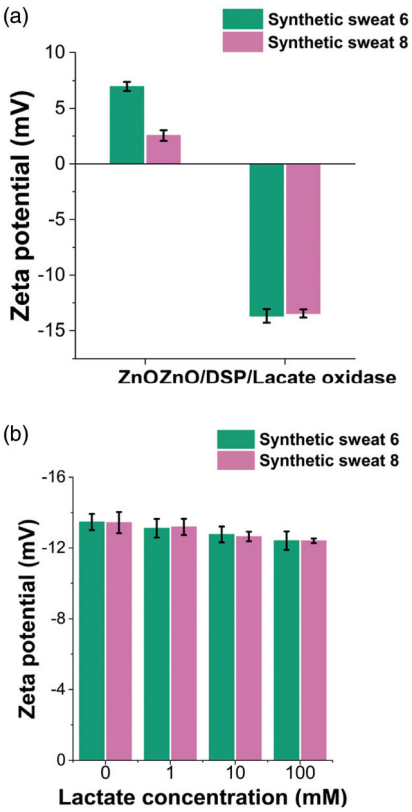

Fig. 4 (a) Zeta potential of bare ZnO and linker (DSP)–enzyme (LOx) modified ZnO nanoparticles in synthetic sweat of pH 6 and 8. (b) Zeta potential response of the enzyme functionalized ZnO nanoparticles to increasing lactate dose concentrations in synthetic sweat of pH 6 and 8.

2.3. Zeta potential analysis for the investigation of enzymatic assay stability in varying sweat pH buffers

The zeta potential quantifies the effective electric charge present on the surface of a particle. We utilize zeta potential measurements to characterize the electrical double layer formed at the sensing element–sweat interface and the modulations arising at the interface due to the LOx–lactate interaction. The surface charge states of a particle suspended in a solution are highly dependent on factors such as varying pH values, ionic strengths, and temperatures. The zeta potentials of bare ZnO nanoparticles and DSP–LOx functionalized ZnO nanoparticles in contact with the sweat of pH 6 and pH 8 are shown in Fig. 4a. The zeta potentials of bare ZnO nanoparticles in the sweat of pH 6 and pH 8 are 6.9 ± 0.4 mV and 2.55 ± 0.5 mV, respectively. Higher potential is observed for ZnO particles suspended in the sweat of pH 6 than pH 8 due to the excess H^+ ions of the sweat buffer surrounding the ZnO nanoparticles. After DSP–LOx functionalization, the zeta potentials in the sweat of pH 6 and pH 8 alter to −13.68 ± 0.6 mV and −13.45 ± 0.3 mV, respectively. The zeta potentials of DSP–LOx modified ZnO nanoparticles in varying pH sweat buffers change to negative potentials from the positive potentials of bare ZnO nanoparticles. At pH 6 and 8, the positive surface charge of ZnO nanoparticles favours electrostatic coupling of the negatively charged enzymes to its surface.[30] Fig. 4b shows the zeta potential response of the enzyme functionalized ZnO nanoparticles to increasing lactate dose concentrations in the sweat buffer of pH 6 and 8. The zeta potentials of zero doses for the sweat of pH 6 and 8 were −13.46 ± 0.45 mV and −13.44 ± 0.6 mV, respectively. For 1 mM lactate concentration, the zeta potentials for the sweat of pH 6 and 8 are observed to be −13.11 ± 0.52 mV and −13.2 ± 0.45 mV, respectively. At 100 mM lactate concentration, the zeta potentials for the sweat of pH 6 and 8 increase to −12.41 ± 0.52 mV and −12.39 ± 0.12 mV, respectively. In the sweat of pH 6 and 8, the zeta potentials tend to become less negative with increasing lactate concentrations due to the production of pyruvic acid making the sweat buffer environment more acidic. The results obtained from the zeta analysis indicate successful immobilization of enzymatic assay chemistry on the ZnO surface and exhibit a pH-stable performance.

2.4. Electrochemical characterization of the lactate biosensing platform for analytical performance evaluation in synthetic and human sweat

Electrochemical impedance spectroscopy has increasingly gained interest in characterizing protein–protein interactions in complex biological matrices. EIS has several advantages such as high sensitivity, non-destructive sensing, quantification of the signal registered due to protein interactions from the background noise produced by the complex biological medium, and the capability to discriminate between interfacial and bulk processes.[31] Herein, the impedance spectrum is recorded within a narrow frequency range by applying a small

AC perturbation signal and then measuring the AC current produced by the electrochemical changes occurring from the immobilized biorecognition element–target analyte interactions. The data extracted from the EIS analysis can be mapped to distinct frequency regimes consisting of solution resistance (R_s), resistance to charge transfer between the electrode surface and the solution (R_{ct}), resistance to diffusion of species to and from the bulk solution (Z_w), and the double layer capacitance (C_{dl}). The numerical values of these individual frequency-dependent impedance parameters can be extracted by fitting the EIS spectrum to the Randle's equivalent circuit [see ESI Fig. S2†]. We have used the non-faradaic mode of EIS for reporting the LOx enzyme–lactate interactions wherein the ionic charges are confined to the electrode and no true charge transfer is observed at the electrode–electrolyte interface making the system more capacitive in nature.[32] The formation of an electrical double layer at the electrode–electrolyte interface is the origin of capacitance in the system. Adsorption of the biorecognition element and its interaction with the target analyte induce a change in the dielectric properties at the electrode–electrolyte interface by displacing water and hydrated ions from the near vicinity, or from the changes in the protein structure conformation which are detected through capacitance probing. The total double layer capacitance of the system is generated from the capacitances contributed by the semiconducting film, the biorecognition element film, and the target analyte–biorecognition element interactions.

Although, human subject testing is considered an ideal validation for performance testing of the lactate detection platform, constraints such as variation in the sweating mechanism, sweat collection times and regions in the same subjects can affect the repeatability in measurements during the system development and characterization phase of the platform. Hence, synthetic sweat is utilized to standardize the sensing protocol and expedite the development of the platform. We have calibrated the performance of the lactate detection platform for increasing lactate concentrations of 0.1–100 mM in synthetic sweat of pH 6 and 8 to understand the effect of sweat pH variance on lactate biosensing. The impedance response is represented as the change in impedance at a given concentration from the baseline impedance at zero dose (sweat devoid of lactate). The percentage change in impedance for increasing lactate dose concentration spiked in sweat is represented by the following equation:

$$\%\,\text{change in impedance} = 100 \times ((Z_{\text{baseline}} - Z_{\text{dose}})/Z_{\text{baseline}}).$$

The signal detection frequency was chosen to be 10 Hz as the maximum signal to noise response was obtained within the 1–100 Hz regime with stable noise variation. The percentage change in impedance for lactate spiked in synthetic sweat of pH 6 (SS6) from 0.1 mM to 100 mM varied from 4.5 ± 2.2% to 37.6 ± 3.3% as shown in Fig. 5a. The specific signal threshold (SST) calculated using an SNR of 3 was computed to

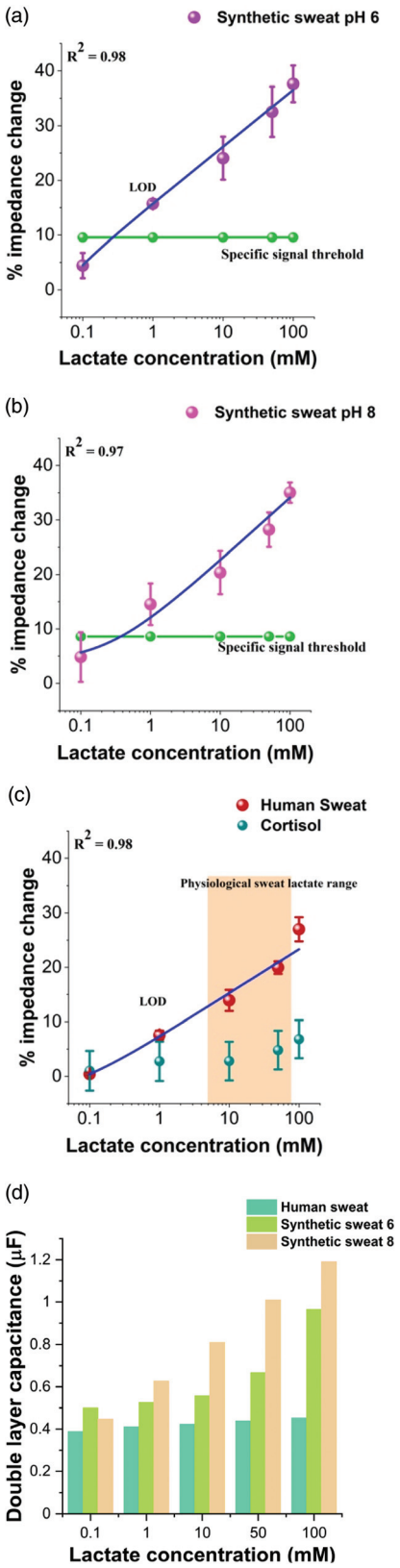

Fig. 5 (a) Calibration dose response of lactate in synthetic sweat of pH 6. (b) Calibration dose response of lactate in synthetic sweat of pH 8. (c) Calibration dose response of lactate in human sweat. (d) Extracted double layer capacitances for 0.1 mM–100 mM lactate concentrations in synthetic sweat of pH 6 and 8, and human sweat.

be 9.5%. The limit of detection of lactate in synthetic sweat of pH 6 was found to be 1 mM with an R^2 of 0.98. The percentage change in impedance for lactate spiked in synthetic sweat of pH 8 from 0.1 mM to 100 mM varied from 4.8 ± 4.5% to 35.1 ± 1.8% as shown in Fig. 5b. The limit of detection was found to be 1 mM as the percentage impedance change recorded from 0.1 mM lactate in synthetic sweat of pH 8 falls under the 8.6% signal threshold level. The coefficient of determination R^2 was found to be 0.97. The dynamic range for lactate detection in synthetic sweat of pH 6 and 8 was found to be 1 mM to 100 mM. The overall percentage change in impedance for lactate dose concentrations in synthetic sweat of pH 6 and 8 varies between ±1 and 4%. The Nyquist plots for the target lactate dose concentration range of 0.1–100 mM spiked in synthetic sweat of pH 6 and 8 are shown in ESI Fig. S3a and S3b†, respectively. The imaginary impedance increases concomitantly with increasing lactate concentrations resulting from the charge storage capacitive properties of the double layer. These modulations arise from the permittivity changes within the double layer which quantifies the LOx enzyme–lactate interactions at the electrode–sweat electrolyte interface and can be validated from the extracted capacitance values obtained from fitting the experimental Nyquist plot to the Randle's circuit as shown in Fig. 5d. The double layer capacitance values demonstrate a dose-dependent increase in response to increasing lactate concentrations. For 0.1 mM to 100 mM lactate dose concentrations, the C_{dl} values vary from 0.5 μF to 0.96 μF for synthetic sweat of pH 6 and 0.44 μF to 1.2 μF for synthetic sweat of pH 8. Fig. 5c shows the calibration dose response curve for the detection of lactate in human sweat. The variation in percentage change in impedance from 0.1 mM to 100 mM lactate concentrations was found to be from 0.4 ± 0.28% to 27 ± 2.2%. The sensitivity of the biosensor is calculated to be 8.3 ± 0.92%/mM. The selectivity of the immobilized LOx enzyme in specifically detecting lactate molecules specifically in a complex human bodily fluid was established through cross-reactivity studies. The cross-reactive study was performed with cortisol as the detection molecule on the lactate biosensing platform. The percentage change in impedance obtained from the cross-reactive interactions of cortisol with the LOx enzyme was found to be from 1.1 ± 3.6% to 6.8 ± 3.4% for cortisol concentrations from 0.1 mM to 100 mM. The impedance responses obtained from 0.1 mM lactate and cortisol overlap while the responses obtained from non-specific cortisol concentrations from 1 mM to 100 mM lie below the responses obtained from specific lactate interactions giving a confirmation that the developed enzymatic assay is specific to the target analyte lactate. The signal threshold was calculated to be 4.3% and the smallest detectable lactate concentration (LOD) was found to be 1 mM making the biosensor capable of detecting lactate within the established physiologically relevant range of 4–80 mM in human sweat.[33] The Nyquist plot for increasing lactate dose concentrations in human sweat is shown in ESI Fig. S3c.† The extraction of double layer capacitance varies from 0.38 μF to 0.46 μF for lactate dose concentrations from 0.1 mM to 100 mM as shown in Fig. 5d. The variations in charge transfer resistance resulting from the increased lactate binding in synthetic sweat of varying pH values and human sweat are shown in ESI Fig. S3d.† The performance calibration outcomes of the lactate biosensing platform demonstrate reliable and specific detection of lactate within the physiologically relevant range present in human sweat primarily originating from the permittivity changes within the double layer. The enhanced sensitivity of detection can be attributed to the nanoporosity of the flexible membrane used for detection which influences transport kinetics, reduces the diffusion time, and provides a high surface area to volume ratio. The macromolecular confinement stabilizes protein, retains protein conformation, and enhances protein–bioreceptor interactions. Selectivity is achieved by leveraging the size-based exclusion feature of the membrane that rejects the interfering lipids and ions present in human sweat allowing for small molecule detection.[34]

2.5. Sensor stability and continuous lactate monitoring

Majority of the biosensing platforms suffer from instability as the immobilized proteins or enzymes are liable to undergo alterations under inappropriate storage conditions further affecting the biosensor's sensitivity. The evaluation of the biosensor's stability is crucial for the assessment of its performance metric particularly in the use of single-use, disposable sensors. The stability metric gauges the retainment of the biosensor's activity when stored under specific conditions to avoid performance degradation.[35] The biosensor strips were immobilized with the LOx enzyme at room temperature and the performance of the lactate biosensor stored at 4 °C until use was measured over 4 days as shown in Fig. 6a. Every day a new biosensor strip was taken out from 4 °C to measure the impedance response of varying lactate concentrations spiked in human sweat. The mean % impedance changes produced over 4 days for 1, 10, and 100 mM lactate concentrations were found to be 11.9 ± 0.96, 18.4 ± 2.05, and 27.0 ± 2.0, respectively. The lactate biosensor's performance decreased by ~30% over the 4-day period while the % coefficient of variation in this duration was computed to be well within 20% variation limit as set by CLSI standards indicating stable sensor operation.

It is imperative to understand the long-term sensing performance of the biosensing platform making it essential to establish the passive sweat patterns in average people during sedentary phases. The average passive sweating rate of one consenting sedentary subject was recorded using a commercial sweat rate sensor (VapoMeter, Delfin Technologies, Ltd) over a 60-minute duration. The average passive sweat rate in the sedentary phase was found to be 19.7 ± 3.2 g m^{-2} h^{-1} as shown in the inset of Fig. 6b. The passive sweat volumes calculated from the sweat rates of the three subjects are calculated to be 0.03–0.05 μL cm^{-2} min^{-1}. Considering a sweat gland density of ~200 cm^{-2} present on the forearm, the passive sweat volume rates can be translated into 3–6 μL sweat volume which is adequate for on-demand, single-use biosensing. The

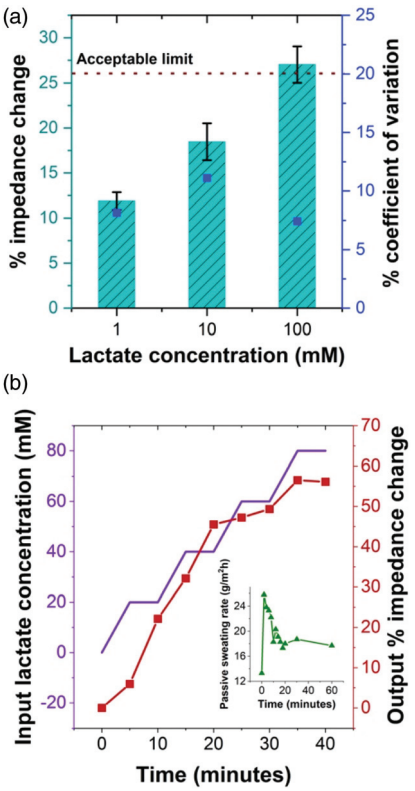

Fig. 6 (a) Stability performance of the lactate biosensing platform over a 4-day duration. The dashed line at 20% represents the acceptable variation limit as set by CLSI standards. (b) Continuous detection of lactate in passively expressed human sweat. The inset shows the passive sweat evaporation pattern in an average person during a sedentary phase.

response of the platform to continuous benchtop dosing of lactate spiked in human sweat to mimic the continuous mode of passive sweat based-lactate detection in real-time is shown in Fig. 6b. The biosensor was dosed with 3 μL lactate concentration in the range of 20–80 mM in a 5-minute loading interval with an incremental percentage change in impedance observed for every dose loading step. The output percentage impedance increases from 5 to 22%, 32 to 45%, and 47 to 49% for 20, 40, and 60 mM lactate loading, respectively. At 80 mM, the sensor begins to reach an inflection point at 56% owing to excess lactate ions causing charge screening. The developed lactate biosensing platform is responsive to accumulative lactate concentrations up to 80 mM in passive human sweat over a 45 min duration before the sensor begins to show signs of saturation.

2.6. Human subject on-demand evaluation of the lactate biosensing platform

The translation of the lactate biosensing platform from a benchtop environment to its utility as an on-demand platform for sedentary lifestyle can be studied by characterizing its performance when placed in close proximity to the human epidermis such that there is direct interaction with the sweat biomarker of interest. The underlying idea is to capture the temporal dynamics of sedentary lifestyle in its entirety from an inactive state to a less active state yet producing passive sweat. The electrochemical performance of the developed lactate biosensor was evaluated to estimate the lactate levels from three consenting human subjects recruited as per IRB compliant protocols. Eccrine sweat glands play an important role in thermoregulating the temperature of the body when sweat is produced in response to activity. The density of the eccrine gland present in the forearm region is 225 ± 25 glands per cm^2 and is chosen to be an ideal location for placing the sensor.[36] The lactate levels were extracted after a 60-minute duration of being sedentary or a lightly intense active phase by correlating the obtained impedances to the impedance ranges obtained from the constructed calibration dose response curves (see the Materials section for the detailed protocol). Signals generated from the interaction of the lactate produced in human eccrine sweat with the LOx enzymatic assay are authenticated by simultaneously testing for lactate on a control sensor without any LOx functionalized on it. Fig. 7a shows the impedance values extracted from the human subjects before and after activity on the LOx functionalized and control sensors, respectively. The impedance responses generated before and after activity from the catalytic interaction of the lactate produced in human sweat with the LOx enzyme lie within the ranges of

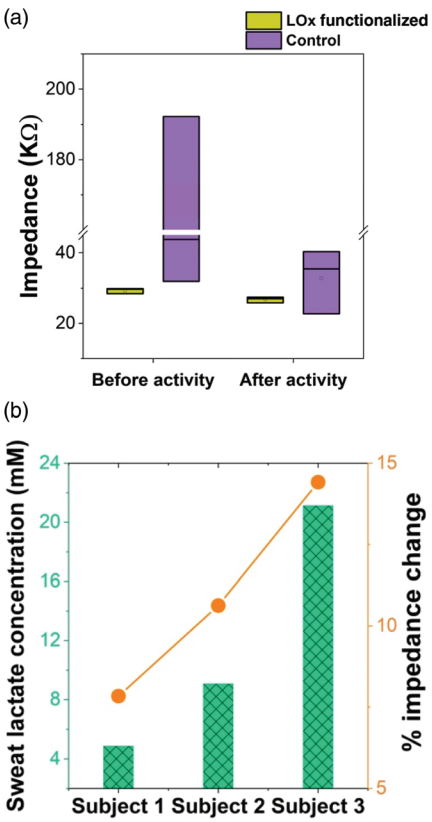

Fig. 7 (a) Extracted impedance values from human subjects before and after activity on LOx functionalized and control sensors. (b) Sweat lactate levels of human subjects extracted after activity on LOx functionalized sensors.

Table 1 Summary of the activity of the human subjects and the ranges of their vital parameters

Subject 1	Sedentary
Subject 2	Sedentary
Subject 3	Light activity
Heart rate	110–120 bpm
Temperature	36–37.5 °C
spO_2	95–100%
Blood pressure	120/80–135/80

28.5–29.5 KΩ and 26.9–27.4 KΩ, respectively, while the impedance ranges produced by the control sensor before and after activity are found to be 44–193 KΩ and 23–41 KΩ, respectively. Additionally, the transition in the phase response from a resistive phase angle prior to activity to a capacitive phase angle post activity confirms our claim of double layer capacitance modulation occurring during the enzymatic catalysis of lactate [see ESI Fig. S4a–c†]. A significant difference is found in the impedance levels presented by the pre- and post-activities of the lactate sensor with a p-value of 0.017 (assuming $p < 0.05$). The decrease in the impedance after the catalytic interaction of the lactate with the LOx enzyme corroborates with our observations made in human sweat calibration studies. The percentage changes corresponding to the extracted sweat lactate levels produced by the lactate sensor lie within the 10–18% range. As shown in Fig. 7b, the sweat lactate levels extracted from the percentage impedance changes observed on the LOx functionalized sensors for subjects 1, 2, and 3 were found to be 4.87 mM, 9.07 mM, and 21.2 mM, respectively, validating the catalysis of sweat lactate by the immobilized LOx on the sensor surface. The responses generated by the enzymatic and non-enzymatic control sensors indicate that the biosensing platform is selective to detecting only lactate present in sweat over other sweat constituents. Table 1 provides the detailed summary about the activity of the human subjects and the ranges of their vital parameters. Factors that affect the sweat lactate production in human subjects depend on the sweat rates, intensity of the exercise, lactate excretion, and the heart rate.[37]

3. Experimental section

3.1. Materials and reagents

Polyamide substrates of pore size 200 nm and thickness 60 μm were obtained from GE Healthcare Life Sciences (Piscataway, NJ, USA). The linker molecule dithiobis succinimidyl propionate (DSP), dimethyl sulfoxide (DMSO), and 1× phosphate buffered saline (PBS) were purchased from Thermo Fisher Scientific Inc. (Waltham, MA, USA). Sodium L-lactate (~98% purity) and ZnO nanopowder (<100 nm) were purchased from Sigma-Aldrich (St Louis, MO, USA). Lactate oxidase (80 U mg^{-1}) was purchased from Toyobo USA. α-Cortisol antibody and hydrocortisone were purchased from Abcam (Cambridge, MA, USA). Synthetic sweat was prepared from the method described in M. T. Mathew *et al.*[38] The pH range was adjusted by varying the concentrations of lactic acid and ammonia. Single donor human sweat of pH ~6 was purchased from Lee Biosolutions Inc. (Maryland Heights, MO, USA). No preservatives were added to this product and it was stored at −20 °C. All lactate dilutions were made in synthetic sweat of pH 6 and 8, and in human sweat.

3.2. Sensor fabrication

The fabrication process of the lactate biosensor involves thin film deposition of 150 nm thick gold interdigitated electrodes on a flexible nanoporous polyamide membrane using a Temescal e-beam evaporator tool (Ferrotec, Livermore, CA, USA). Further, a 100 nm thick semi-conducting ZnO thin film was sputtered onto the overlap region between the interdigitated gold electrodes using AJA Orion RF magnetron with a 99.999% ZnO target (Kurt J. Lesker, Pittsburgh, PA, USA).

3.3. Lactate biosensor calibration

3–5 μL volume of 10 mM DSP linker was diluted in DMSO and incubated on the sensor surface for 3 hours. All solutions are dispensed from the backside of the sensor. 3–5 μL PBS wash was carried out to remove any unbound linker. The linker functionalized surface was treated with 4 mg ml^{-1} of lactate oxidase and incubated for 90 minutes. The lactate-free synthetic sweat was applied to the sensing region to obtain baseline impedance measurement. Furthermore, lactate dilutions of concentrations of 0.1, 1, 10, 50, and 100 mM were made in synthetic and human sweat buffers. The lactate doses were incubated on the sensor surface for 5 minutes to allow for the catalysis reaction to occur. The lactate doses were applied serially from low to high concentrations to construct the calibration response curve. The cross-reactivity study was performed in a similar manner with cortisol dose concentrations of – 0.1, 1, 10, 50, 100 mM made in human sweat buffer being introduced serially on the sensing surface. EIS measurements were performed using a potentiostat (Gamry Instruments, Warminster, PA, USA) after the application of a 10 mV AC excitation signal with a frequency sweep of 1 Hz to 1 MHz. All measurements were carried out under ambient temperature conditions. All data are represented as mean ± relative standard deviation (RSD). A sample set of n = 3 was used throughout this research for building CDRs in synthetic and human sweat buffers.

The stability study was performed by immobilizing the lactate oxidase enzyme on four sensors and storing it at 4 °C until use. Each day a new sensor was tested by serially applying 1, 10, and 100 mM lactate doses made in human sweat and EIS measurements were recorded at 10 Hz.

The continuous dosing study was performed by dispersing 20, 40, 60, and 80 mM lactate doses made in human sweat on the sensor successively. Each lactate dose concentration was added twice at the rate of 3μL every 5 minutes over a total duration of 45 minutes. Single frequency EIS response was recorded at 10 Hz.

3.4. ATR-IR spectroscopy

The infrared spectra collected to establish the successful functionalization of the lactate detection enzymatic assay were

recorded using a Thermo Scientific Nicolet iS-150 FTIR spectrometer (Waltham, MA, USA) in Attenuated Total Reflectance (ATR) mode. The tool consists of a KBr window and a deuterated triglycine sulphate (DTGS) detector. A Harrick VariGATR sampling stage with a 65° germanium crystal was used to obtain the spectra. The spectra were collected with a resolution of 4 cm^{-1} for 256 scans in a wavelength range of 4000 cm^{-1} to 600 cm^{-1}. The ATR-IR samples were prepared on a ZnO deposited polyamide membrane by functionalizing the lactate detection enzymatic assay.

3.5. X-Ray photoelectron spectroscopy

XPS spectra were recorded using a PHI 5000 Versa Probe II (ULVAC-PHI, Inc., Methuen, MA, USA) with monochromatic Al Kα radiation ($h\nu$ = 1486.6 eV) at a 45° takeoff angle with respect to the sample surface. All spectra were obtained with a 0.2 eV step size and a 23.50 eV pass energy. The base pressure in the analysis was maintained at 1.6×10^{-8} Torr. Sample preparation was carried out on a silicon wafer by functionalizing the lactate detection enzymatic assay. Furthermore, the prepared samples were dried in a vacuum chamber. All binding energies were corrected for the charge shift using the C1 s peak of graphitic carbon (BE = 284.8 eV) as a reference.

3.6. Zeta potential study

Zeta potential measurements were carried out in synthetic sweat of pH 6 and 8 to validate the enzymatic assay functionalization on the ZnO sensing surface using Malvern ZetaSizer Nano ZS (Malvern Panalytical, Malvern, UK). The zeta potential was calculated from the measured electrophoretic mobility using the Smoluchowski approximation:

$$\mu = (\varepsilon \times \zeta)/\eta$$

where μ is the electrophoretic mobility; ε is the dielectric constant; ζ is the zeta potential; and η is the viscosity of solution. Initially, the zeta potentials of the zinc oxide nanoparticles suspended in synthetic sweat of pH 6 and 8 were measured. Furthermore, 10 μL of ZnO nanoparticles, 10 μL of DSP made in DMSO, and 10 μL of lactate oxidase enzyme were incubated for three hours at room temperature followed by the addition of 970 μL of synthetic sweat of pH 6 and 8. All measurements were performed in triplicate. The zeta potentials for lactate concentrations of – 0, 1, 10, and 100 mM made in synthetic sweat of pH 6 and 8 were recorded to ensure the functionality of the enzymatic assay immobilized on the ZnO surface.

3.7. Vapometer sweat rate measurements

One healthy volunteer (age: 20–30 years) was recruited for sweat rate measurement study using an FDA approved commercial device VapoMeter (Delfin Technologies, Ltd, Kuopio, Finland) that measures the transepidermal water loss and the sweat evaporation rate. The subject was asked to wear a trimmer band on the forearm at the site of sweat rate measurement to induce passive sweat. Measurements were carried out every 2 minutes for 60 minutes. Written and informed consent was obtained from the subject prior to the study. All trials were conducted with strict compliance to the IRB protocol (#19–23) approved by the Institutional Review Board of University of Texas at Dallas.

3.8. Human subject testing

Three healthy volunteers (age: 20–30 years) were recruited for this study. Written and informed consent was obtained from the subjects prior to the study. All trials were conducted with strict compliance to the IRB protocol (#18–116) approved by the Institutional Review Board of University of Texas at Dallas. The study conducted involves less than minimal risk. The recruited volunteers had no history or existing heart conditions, diabetes, or muscular pain. The site of sensor placement on the forearm was cleaned with alcohol wipes prior to securing the control and the LOx functionalized sensors with a medical grade adhesive. The volunteers were asked to wear a trimmer belt on their arm to induce sweating for the 60-minute duration of being sedentary or during the light activity phase. The impedance baselines of the control and LOx functionalized sensors were measured prior to human subject trials. After the 60-minute duration, the sweat lactate levels were determined by connecting the sensor to the Gamry for impedance measurements. The instantaneous lactate levels were calculated by measuring the percentage change in impedance before and immediately after 60 minutes. The sensors were carefully unmounted from the forearm of the volunteers and the impedance data were recorded using a potentiostat (Gamry Instruments, Warminster, PA, USA) at 10 Hz frequency.

4. Conclusions

The timely recognition of diseases by means of non-invasive fluids such as eccrine sweat would be critical in providing rapid treatment and improving the survival rates for patients that further develop complications. The design and development of on-demand, point-of-use sensing platforms will aid in the measurement of biomarker levels for better care of sedentary population. Lactate detection has grown out of the stage of infancy to become a molecule of interest in health and disease monitoring. Emergent flexible sensing technologies have shifted their focus from fitness tracking towards real-time physiological biomarkers in non-invasive bodily fluids for disease detection. Aside from being a workhorse biomarker for endurance testing in the sports arena, increased lactate production is indicative of clinical conditions caused by restricted oxygen supply. The key highlight of this work is the epidermal functionality and performance of a sweat lactate sensor on a surface engineered nanoporous platform with low volume detection capability for on-demand measurements. The semiconducting properties of nanotextured zinc oxide films have been leveraged for the sensitive detection of lactate in a complex human sweat buffer through the non-faradaic EIS technique. EIS gives a microscopic understanding of the enzyme–target analyte interaction dynamics characterized by

the charge perturbations occurring in the double layer. The lactate biosensor exhibited an LOD of 1 mM and a dynamic detection range of 1–100 mM in human sweat. A highly specific response to lactate was observed with minimal cross-reactivity from the non-specific molecules present in human sweat. Stability and continuous dosing studies indicate the robustness and the long-term capability of the biosensing platform in detecting lactate in human sweat. The on-demand feature of the biosensing platform provided a rapid quantification of sweat based-lactate levels when placed on human subjects. ATR–FTIR and XPS analyses give a confirmation on the enzymatic assay immobilization on the ZnO sensing surface. The modification in the surface charge at the electrode–electrolyte interface as a consequence of enzymatic assay binding and synergistic interactions between enzyme–lactate is characterized by the zeta potential.

Conflicts of interest

Drs Shalini Prasad and Sriram Muthukumar have significant interest in Enlisense LLC, a company that may have commercial interest in the results of this research and technology. The potential individual conflict of interest has been reviewed and managed by The University of Texas at Dallas, and played no role in the study design; in the collection, analysis, interpretation of data; in the writing of the report, or in the decision to submit the report for publication.

Acknowledgements

The authors would like to thank John Craven for helping with the scanning electron micrographs.

References

1 D. Hashoul and H. Haick, *Eur. Respir. Rev.*, 2019, 28.
2 A. Gholizadeh, D. Voiry, C. Weisel, A. Gow, R. Laumbach, H. Kipen, M. Chhowalla and M. Javanmard, *Microsyst. Nanoeng.*, 2017, **3**, 1–8.
3 A. Shalaby, O. Khalafallah, M. Galal, H. H. Assal and N. Ahmed, *Egypt. J. Chest Dis. Tuberc.*, 2016, **65**, 695–700.
4 S. Jadoon, S. Karim, M. R. Akram, A. Kalsoom Khan, M. A. Zia, A. R. Siddiqi and G. Murtaza, *Int. J. Anal. Chem.*, 2015, hindawi.com.
5 B. A. Katchman, M. Zhu, J. Blain Christen and K. S. Anderson, *Proteomics: Clin. Appl.*, 2018, **12**(6), 1800010.
6 J. N. Hussain, N. Mantri and M. M. Cohen, *Clin. Biochem. Rev.*, 2017, **38**(1), 13.
7 K. Mitsubayashi, M. Suzuki, E. Tamiya and I. Karube, *Anal. Chim. Acta*, 1994, **289**, 27–34.
8 M. J. Buono, N. V. L. Lee and P. W. Miller, *J. Physiol. Sci.*, 2010, **60**, 103–107.
9 J. M. Green, R. C. Pritchett, T. R. Crews, J. R. McLester and D. C. Tucker, *Eur. J. Appl. Physiol.*, 2004, **91**, 1–6.
10 X. Cai, J. Yan, H. Chu, M. Wu and Y. Tu, *Sens. Actuators, B*, 2010, **143**, 655–659.
11 W. Jia, A. J. Bandodkar, G. Valdés-Ramírez, J. R. Windmiller, Z. Yang, J. Ramírez, G. Chan and J. Wang, *Anal. Chem.*, 2013, **85**, 6553–6560.
12 W. Gao, S. Emaminejad, H. Y. Y. Nyein, S. Challa, K. Chen, A. Peck, H. M. Fahad, H. Ota, H. Shiraki, D. Kiriya, D.-H. Lien, G. A. Brooks, R. W. Davis and A. Javey, *Nature*, 2016, **529**, 509–514.
13 P. J. Derbyshire, H. Barr, F. Davis and S. P. J. Higson, *J. Physiol. Sci.*, 2012, **62**, 429–440.
14 K. C. Lin, S. Muthukumar and S. Prasad, *Talanta*, 2020, **214**, 120810.
15 W. Jia, A. J. Bandodkar, G. Valdés-Ramírez, J. R. Windmiller, Z. Yang, J. Ramírez, G. Chan and J. Wang, *Anal. Chem.*, 2013, **85**, 6553–6560.
16 T. Terse-Thakoor, M. Punjiya, Z. Matharu, B. Lyu, M. Ahmad, G. E. Giles, R. Owyeung, F. Alaimo, M. Shojaei Baghini, T. T. Brunyé and S. Sonkusale, *npj Flexible Electron.*, 2020, **4**, 1–10.
17 R. Wang, Q. Zhai, T. An, S. Gong and W. Cheng, *Talanta*, 2020, 121484.
18 L. Zhang, J. Liu, Z. Fu and L. Qi, *J. Nanosci. Nanotechnol.*, 2019, **20**, 1495–1503.
19 Q. Zhang, D. Jiang, C. Xu, Y. Ge, X. Liu, Q. Wei, L. Huang, X. Ren, C. Wang and Y. Wang, *Sens. Actuators, B*, 2020, **320**, 128325.
20 M. E. Payne, A. Zamarayeva, V. I. Pister, N. A. D. Yamamoto and A. C. Arias, *Sci. Rep.*, 2019, **9**, 1–10.
21 J. H. Bae, J. H. Han and T. D. Chung, *Phys. Chem. Chem. Phys.*, 2012, **14**, 448–463.
22 S. Prasad, A. P. Selvam, R. K. Reddy and A. Love, *J. Lab. Autom.*, 2013, **18**, 143–151.
23 A. P. Minton, *Biophys. J.*, 2005, **88**(2), 971–985.
24 I. M. Kuznetsova, K. K. Turoverov and V. N. Uversky, *Int. J. Mol. Sci.*, 2014, **15**, 23090–23140.
25 S. Upasham, K. Thai, R. Muthyala and S. Prasad, *Analyst*, 2020, **145**, 784–796.
26 N. Tripathy and D. H. Kim, *Nano Convergence*, 2018, **5**, 1–10.
27 S. K. Arya, S. Saha, J. E. Ramirez-Vick, V. Gupta, S. Bhansali and S. P. Singh, *Anal. Chim. Acta*, 2012, **737**, 1–21.
28 A. Bhide, S. Muthukumar and S. Prasad, *Biosens. Bioelectron.*, 2018, **117**, 537–545.
29 R. D. Munje, M. Jacobs, S. Muthukumar, B. Quadri, N. R. Shanmugam and S. Prasad, *Anal. Methods*, 2015, **7**, 10136–10144.
30 N. Wiesmann, W. Tremel and J. Brieger, *J. Mater. Chem. B*, 2020, **8**, 4973–4989.
31 A. Bogomolova, E. Komarova, K. Reber, T. Gerasimov, O. Yavuz, S. Bhatt and M. Aldissi, *Anal. Chem.*, 2009, **81**, 3944–3949.
32 B. L. Garrote, A. Santos and P. R. Bueno, *ACS Sens.*, 2019, **4**, 2216–2227.

33 D. A. Sakharov, M. U. Shkurnikov, M. Y. Vagin, E. I. Yashina, A. A. Karyakin and A. G. Tonevitsky, *Bull. Exp. Biol. Med.*, 2010, **150**, 83–85.
34 J. I. Njagi and S. M. Kagwanja, in *ACS Symposium Series*, American Chemical Society, 2011, vol. 1062, pp. 225–247.
35 T. D. Gibson, *Analusis*, 1999, **27**, 630–638.
36 M. Harker, *Skin Pharmacol. Physiol.*, 2013, **26**, 92–100.
37 L. B. Baker, *Temperature*, 2019, **6**, 211–259.
38 M. T. Mathew, E. Ariza, L. A. Rocha, A. C. Fernandes and F. Vaz, *Tribol. Int.*, 2008, **41**, 603–615.